Article

Not peer-reviewed version

Luminescent Nanoparticles of $Gd_2O_3:Eu^{3+}$ Encapsulated Within SiO_2-PMMA Gel-Polymer Hybrid Matrix: Synthesis and Optical Properties

Martin Rodolfo Palomino Merino *, Juan de la Cruz Quiroga, Oliver Isac Ruiz Hernández, Oscar Mario Martínez Bravo, Benito de Celis Alonso, Angelica Gutiérrez Franco, Miller Toledo Solano, Claudia Mendoza-Barrera, Humberto Salazar Ibarguen

Posted Date: 6 April 2026

doi: 10.20944/preprints202604.0322.v1

Keywords: sol–gel processes; gel-polymer matrix; hybrid materials; luminescence

 doi:10.20944/preprints202604.0322.v1

Article

Luminescent Nanoparticles of $Gd_2O_3:Eu^{3+}$ Encapsulated Within SiO_2-PMMA Gel-Polymer Hybrid Matrix: Synthesis and Optical Properties

Martin Rodolfo Palomino Merino [1], Juan de la Cruz Quiroga [1], Oliver Isac Ruiz Hernández [1], Oscar Mario Martínez Bravo [1], Benito de Celis Alonso [1], Angélica Gutiérrez Franco [1], Miller Toledo Solano [1], Claudia Mendoza Barrera [1] and Humberto Salazar Ibargüen [1,2]

[1] Facultad de Ciencias Físico Matemáticas, Benemérita Universidad Autónoma de Puebla, Avenida San Claudio y 18 Sur, Colonia San Manuel, Ciudad Universitaria, Puebla 72570, México

[2] Centro Interdisciplinario de Investigación y Enseñanza de la Ciencia (CIIEC), Benemérita Universidad Autónoma de Puebla, C.P. 72570, Puebla, México

* Correspondence: palomino@fcfm.buap.mx

Abstract

Luminescent gadolinium oxide nanoparticles doped with europium were synthesized through a precipitation reaction using gadolinium and europium nitrates as precursors. The europium- doped gadolinium oxide nanoparticles were incorporated first: into a Gel matrix of silicon dioxide; and second: mixing with Polymethyl Methacrylate. Both processes are synthesized by the simultaneous hydrolysis of tetraethyl orthosilicate and polymerization of 3-(Trimethoxysilyl) propyl methacrylate. The solid samples obtained are round in shape with a size of about 2.5 cm, which makes it easy to handle to test different applications. The inclusion of $Gd_2O_3:Eu^{3+}$ nanoparticles increases the level of absorbance in the ultraviolet region, which allows for improved emission of the material at a wavelength of around 609 nm. Furthermore, it enables easy doping of the material and the fabrication of thin films and monoliths with potential optical applications.

Keywords: sol–gel processes; gel-polymer matrix; hybrid materials; luminescence

1. Introduction

Gadolinium oxide (Gd_2O_3) has gained significant interest due to its unique properties, making it useful in several technological applications. It exhibits high transmission in the visible region of the electromagnetic spectrum, a wide bandgap (5.8-6.4 eV), low phonon energy (~600 cm^{-1}), outstanding chemical stability, and a high neutron absorption cross-section [1–3]. These attributes make it useful in semiconductor devices [4], as a phosphor in optoelectronic devices, and for neutron detection and capture. Nanoparticles of Gd_2O_3 possess unique size-dependent properties, and their high surface area allows them for a wide range of applications, including catalysis and molecular sensing [5,6]. Moreover, Gd_2O_3 nanoparticles showcase high biocompatibility [7–9], leading to their remarkable use as a contrast agents in MRI scanning in the medical field [9]. Rare-earth-doped Gd_2O_3 nanoparticles have also demonstrated promising luminescent properties [10–13].

Hybrid materials and nanocomposites have multiple components bonded at the nanometric or molecular level. Technological research has shown that specific properties can be achieved with these materials that otherwise could not be possible with a single component. These hybrid materials often exhibit improved mechanical properties over their individual components [14,15]. Additionally, several properties, such as optical [16,17] and electrical [18,19] characteristics, can be fine-tuned by

 doi:10.20944/preprints202604.0322.v1

changing the ratios and compositions of the components. Notably, particular phosphors retain their luminescent properties while gaining photostability when incorporated into these materials [20–23].

In this work luminescent europium-doped Gd_2O_3 ($Gd_2O_3:Eu^{3+}$) nanoparticles were incorporated into a silica-polymethyl methacrylate (SiO_2-PMMA) hybrid matrix, which was synthesized by sol-gel method. The $Gd_2O_3:Eu^{3+}$ nanoparticles served as phosphorous (Luminescent phosphorus materials) [24] while the SiO_2-PMMA hybrid provided mechanical strength to the material. The resulting luminescent composite can be efficiently used in solid state applications or as thin film, with tunable properties. The optical properties of the composite were analyzed using UV-Vis and photoluminescence spectroscopies. The morphology of the composite was observed through scanning electron microscopy (SEM) and atomic force microscopy (AFM) while its chemical structure was assessed using Raman spectroscopy. Then, the $Gd_2O_3:Eu^{3+}$ nanoparticles and the SiO_2-PMMA hybrid matrix were characterized.

2. Materials

To synthesize nanoparticles, europium (III) nitrate pentahydrate ($Eu(NO_3)_3{\cdot}5H_2O$, 99%), gadolinium (III) nitrate hexahydrate ($Gd(NO_3)_3{\cdot}6H_2O$, 99%), ammonium hydroxide (NH_4OH) were used, with polyvinyl pyrrolidone ($(C_6H_9NO)_n$, 99%) serving as surfactant. In the case of SiO_2-PMMA hybrid material synthesis, tetraethyl orthosilicate ($SiC_8H_{20}O_4$, 98%, TEOS), methyl methacrylate ($C_5H_8O_2$, MMA, 99%), 3-(Trimethoxysilyl) propyl methacrylate ($C_{10}H_{20}O_5Si$, TMSPM, 98%) were used. All reagents were purchased from Sigma-Aldrich and used without further purification. Commercial medical grade distilled water was used for hydrolysis, and ethanol (99.9%, J.T. Baker) acted as the solvent. Benzoyl peroxide ($C_{14}H_{10}O_4$, 98%, Sigma Aldrich) was employed as catalyst, while sodium hydroxide pellets (NaOH, 98%, J.T. Baker) were used to control the pH of the solution.

3. Experimental

The $Gd_2O_3:Eu^{3+}$ nanoparticles were synthesized through a precipitation reaction. Initially, 0.5 g of Gadolinium (III) nitrate hexahydrate ($Gd(NO_3)_3{\cdot}6H_2O$) and 0.01 g of Europium(III) nitrate pentahydrate ($Eu(NO_3)_3{\cdot}5H_2O$) were dissolved in 20 ml of water and stirred for 30 minutes to obtain a homogeneous mixture. Next, 0.5 ml of ammonium hydroxide (NH_4OH) was added drop by drop to the mixture. As the reaction progressed, $Gd(OH)_3$ particles were formed as a white precipitate. Then this precipitate was centrifuged and washed at least three times with distilled water. The product was dried in an oven at 80 °C and treated at 600 °C for 4 hours to obtain Gd_2O_3 particles by the thermal decomposition of the precursors.

The SiO_2-PMMA hybrid was synthesized using the sol-gel technique, which involved the simultaneous hydrolysis of TEOS and the polymerization of MMA in an ethanol solution. TMSPM served as bonding agent between the SiO_2 and the PMMA molecules. The molar proportions used were TEOS: MMA: TMSPM: H_2O: Ethanol in a ratio of 1:1:0.22:4.75:4.75. Benzoyl peroxide was added as a catalyst for the MMA polymerization at a 1% concentration relative to MMA. NaOH was incorporated into the solution to regulate the acidity; an optimal pH between 9 and 10 was determined for the gelation of the sol. To modify the matrix, 20 mg of europium-doped Gd_2O_3 nanoparticles were incorporated into 10 ml of the hybrid sol. The sol was then allowed to gel and dry in a sealed container, which had a small opening to facilitate slow and continuous solvent evaporation.

The samples were characterized by X-ray diffraction. SEM, AFM, Raman, UV-Vis, and photoluminescence spectroscopies. X-Ray diffraction was carried out using the equipment Panalytical Empyrean diffractometer using the Bragg-Brentano configuration and Cu-Kα (1.5406 Å) radiation source with a pass time of 45 s. The surface of the samples was analyzed using a JEOL Scanning Electron Microscope model JSM-5600LV. Raman spectroscopy (LabRAM, Horiba Scientific), with excitation from a HeNe laser at a wavelength of 633 nm from 200-2000 cm^1, was used to study the chemical composition of the samples. A spectrofluorometer (Nanolog, Horiba Scientific),

 doi:10.20944/preprints202604.0322.v1

was utilized to characterize the emission spectra of the samples, using an excitation wavelength of 350 nm. The UV-Vis absorption spectra (Cary 5000, Agilent) were measured through diffuse reflectance. AFM (XE7, Park Systems) micrographs were taken using a tapping mode and a C-soft tapping cantilever (Budget Sensors).

4. Results and Discussion

The analysis of the XRD data, presented in **Figure 1**, confirms that the $Gd_2O_3:Eu^{3+}$ particles have a crystal structure of Gd_2O_3 in the cubic phase, after the heat treatment [25]. The diffraction peaks corresponding to the (211), (222), (400), (431), (440), and (622) planes at 2θ values of 20.12°, 28.69°, 33.18°, 42.64°, 47.65°, and 56.30°. Due to the gadolinium oxide crystallizing in the Ia-3 crystallographic group, the gadolinium ions occupied the C2 and S6 Wyckoff sites in a 3:1 ratio, alongside with europium (III) which served as an active luminescent ion, due to the radius similarity [26]. The average crystallite size of $Gd_2O_3:Eu^{3+}$ particles, calculated using the Scherrer Equation, using an X-ray wavelength of 0.15418 nm, was 21.4 nm.

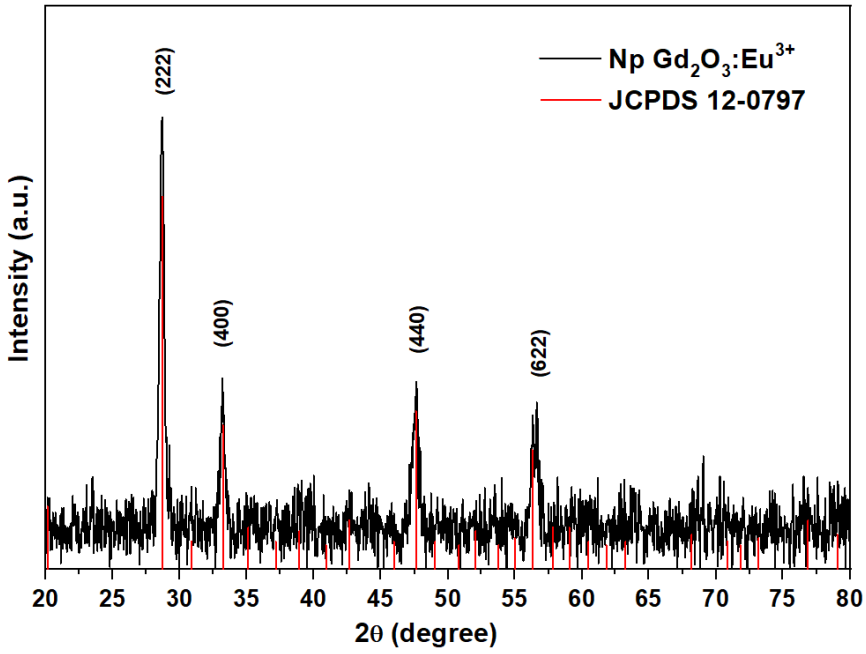

Figure 1. XRD spectra of the $Gd_2O_3:Eu^{3+}$ nanoparticles.

During the fabrication, as the gel dried and shrank, $Gd_2O_3:Eu^{3+}$ particles precipitated creating a luminescent layer at the bottom of the container. The interactions between the hybrid gel and the pressure exerted by the shrinking gel compacted this nanoparticle layer into a solid structure supported by the surrounding matrix. Figure 2 shows SEM images of the nanoparticle layer, where it is appreciated that the material is solid and nonporous. No individual nanoparticles can be observed, indicating that the matrix successfully kept the $Gd_2O_3:Eu^{3+}$ nanoparticles fixed to the substrate. The layer exhibits cracks and irregularities on its surface, likely caused by tensile forces during the shrinking process of the gel as well as differences in the shrinking rates between the layers with low and high nanoparticle concentrations.

 doi:10.20944/preprints202604.0322.v1

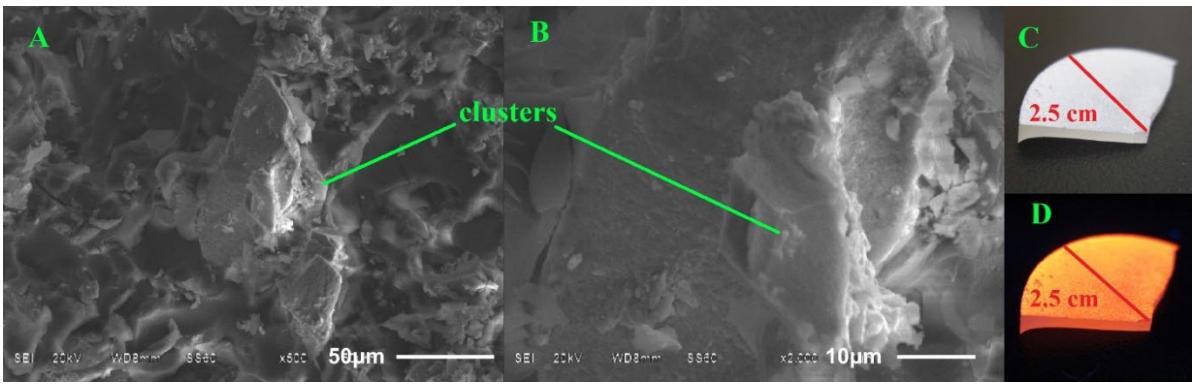

Figure 2. SEM images of the nanoparticle layer on the SiO2-PMMA monolith at **a)** X500 and **b)** X2000. Photograph of a sample monolith with diameter size around 2.5 cm, under **c)** visible light and, **d)** 250 nm UV light.

Images, taken from the low and high concentration layers, using AFM, are presented in Figure 3. In Figure 3(A), it can be observed that the surface of the material presents two distinctive zones, prominent protrusions with sharp edges that stand out the surface and a surrounding smoother material. Figure 3(B) presents an AFM micrograph that focuses on these protrusions, revealing clusters of fused particles with well-defined edges and clear boundaries.

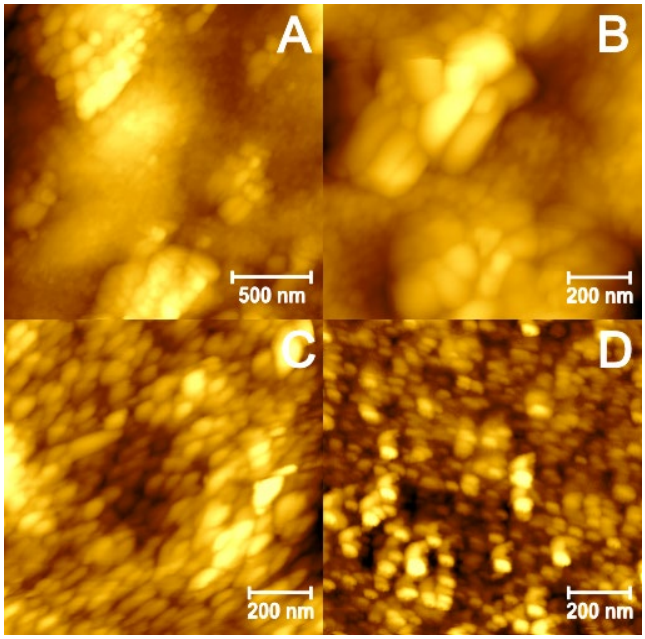

Figure 3. AFM micrographs of the $Gd_2O_3:Eu^{3+}$ nanoparticle layer on the SiO_2-PMMA monolith. **(A)** shows the nanoparticle layer at low magnification, **(B)** centers around a group of clusters, **(C)** focuses on the area between clusters, and **(D)** SiO_2-PMMA layer.

Figure 3(C) shows AFM image of the smooth surface surrounding the clusters, highlighting the contrast in smoothness between the areas of protrusions and the protrusions themselves. Figure 3(D) displays a layer of the SiO_2-PMMA matrix containing a low concentration of $Gd_2O_3:Eu^{3+}$ nanoparticles. The morphologies of the materials in Figure 3(C) and 3(D) are similar, consisting of fused spherical particles. The spherical particles observed in the SiO_2-PMMA layer are identified as SiO_2-PMMA particles formed through the sol-gel process. In contrast, the larger clusters are primarily composed of $Gd_2O_3:Eu^{3+}$ nanoparticles. Since no other compounds were involved in the synthesis of the material, we propose that the PMMA did not integrate into the sol-gel particles but served instead to fill the spaces between the $Gd_2O_3:Eu^{3+}$ particles, providing mechanical support to the lager clusters.

 doi:10.20944/preprints202604.0322.v1

The average diameter of $Gd_2O_3:Eu^{3+}$ particles was found to be 97 ± 54 nm. This measurement was based on an analysis of 950 particles from the AFM micrographs, using ImageJ® and OriginPro® software.

Figure 4 presents the Raman spectra of the SiO_2-PMMA unmodified hybrid and the modified hybrid containing nanoparticles (SiO_2-PMMA+$Gd_2O_3:Eu^{3+}$). The Raman bands identified, and their assignments, are shown in Table 1 [27–34]. When $Gd_2O_3:Eu^{3+}$ nanoparticles are included, a peak appears at 359 cm^{-1}, which corresponds to the Fg mode in the cubic phase of the gadolinium oxide, thus confirming the presence of the nanoparticles within the composite. The addition of the $Gd_2O_3:Eu^{3+}$ nanoparticles did not generate new peaks, indicating that no chemical bonds were formed between the matrix and the nanoparticles. The spectra revealed changes in the relative intensities of the bands between the doped and undoped samples. The peaks observed at 377, 603, 1013, 1048, 1260, 1410, 1450, 1637, and 1764 cm^{-1} are associated with PMMA chains. Variations in the relative strengths of these peaks indicate a change in the degree of polymerization of PMMA and the overall length of the polymer chains.

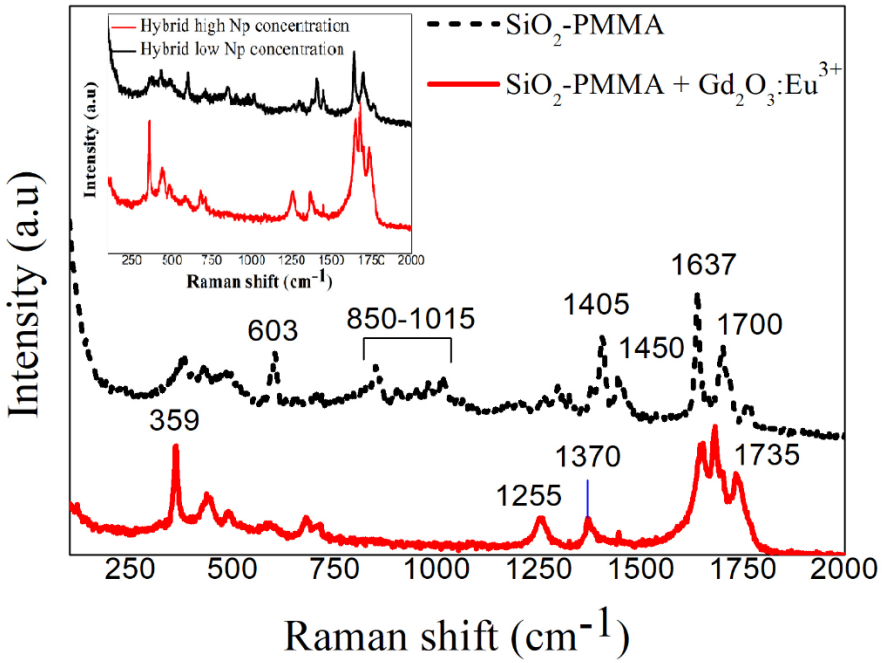

Figure 4. Raman spectra of SiO2-PMMA matrix and SiO2-PMMA-+Gd2O3:Eu3+ composite. Figure Inset: Comparison of Raman spectra between the areas of high and low nanoparticle concentration in each sample.

Table 1. Raman bands and their assignments of samples. The [a-h] assignments match with references [27–34].

Frequency (cm^{-1})	Assignment	Frequency (cm^{-1})	Assignment
359[a]	F_g+A_g	1048[c,h]	ν(C-C)
377[f]	CC[a]C	1265[c]	ν(C-C), ν(C-COO)
433[b]	≥5 fold-ring (ω_1)	1300[d]	Si-CH_3
488[b]	D_1	1328[d,f]	-CH_2
603[b,c]	D_2, ν(C-COO), ν_s(C-C)	1370[d,f]	α-CH_3
661[c]	Si-O-C	1405[d,f]	-CH_3
710[e]	Si-O-C	1450[c,f]	δ_a(C-H) of α-CH_3, δ_a(C-H) of O-CH_3
854[b,c]	Si-O-2NBO stret.	1637[c,d,g]	O-H, ν(C=C), ν(C-COO)
904[b]	Si-O-2NBO stret.	1700[c,g,h]	ν(C=O)
980[b]	Si-OH sym stret.	1735[c,f,h]	ν(C=O)
1015[c,h]	-CH_3		

 doi:10.20944/preprints202604.0322.v1

An increase in the peaks in 1637, 1700, and 1735 cm^{-1} corresponds to an increase in the number of C=O bonds, due to an overall increase in the degree of polymerization of the PMMA and an elongation of the polymer chains. This also explains the reduction in peaks between 1330 and 1450 cm^{-1}, which are associated with -CH_3 and -CH_2 bonds, the terminal points of the polymer chain.

Changes are observed in Raman bands associated with SiO_2, specifically in the 433 and 711 cm^{-1} bands, which are assigned to silica rings and Si-C-O bonds, indicating a decrease in the types of bonds. The disappearance of peaks between 850 and 1015 cm^{-1} indicates a reduction in the presence of non-bridging bonds as well as Si-OH bonds. The increase in the 603 cm^{-1} band is attributed to vibrations of the longer polymer chains and the enhanced crosslinking in the SiO_2 network.

Due to the formation of the two-layers system in the sample, Raman spectra were taken from the high- and low-nanoparticle concentration layers. The inset of Figure 4 presents a comparison of the spectra. It can be observed that the same bands appear in both layers, similar to those in the doped and undoped matrix. The low-concentration layer appears to behave like pure SiO_2-PMMA, as the characteristic Gd_2O_3 peak at 360 cm^{-1} is not detectable. This indicates that this layer contains no measurable amounts of nanoparticles. Additionally, differences in the relative intensities associated with PMMA chains are observed between the low and high nanoparticle concentration layers in the samples. This suggests either a higher amount of polymer or a higher degree of polymerization in the nanoparticle layer. The increased presence of PMMA chains supports the hypothesis that unreacted material from the sol-gel process acts as a binding agent between the nanoparticles.

The UV-Vis absorption spectra presented in Figure 5 demonstrated that the material exhibited high transparency in the visible region of the electromagnetic spectrum, while showing significant absorption in the UV region. The nanoparticles showed a peak around 250 nm, and the hybrid exhibited a similar broader band at the same wavelength. This strong absorption in the hybrid material can be attributed to the presence of PMMA chains, which are known for their high UV absorption capacity [35]. When the nanoparticles are added to the SiO_2-PMMA the overall absorption of the material is increased across the entire UV spectrum. This high level of absorption may hinder the excitation of the luminescent layer through the SiO_2-PMMA layer. However, although the emitted light can be transmitted through all the composites, this characteristic could be advantageous for specific applications, as it allows for directional control over excitation wavelengths. In contrast, the emitted light is able to pass freely through the material.

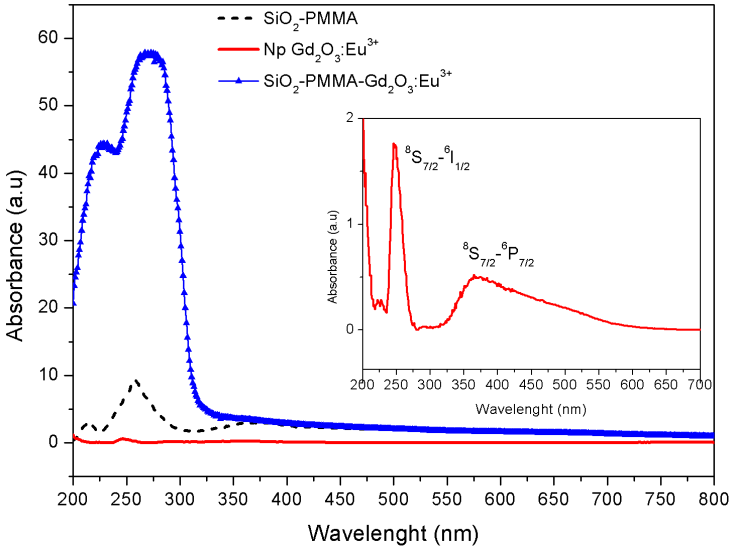

Figure 5. Absorption spectra of the $Gd_2O_3:Eu^{3+}$ nanoparticles, SiO_2-PMMA hybrid material, SiO_2-PMMA matrix with $Gd_2O_3:Eu^{3+}$ nanoparticles (SiO_2-PMMA+$Gd_2O_3:Eu^{3+}$).

 doi:10.20944/preprints202604.0322.v1

In Figure 6, the absorption spectra were analyzed to determine the optical bandgap of the samples using the Tauc's method. The direct bandgap of the $Gd_2O_3:Eu^{3+}$ nanoparticles was 5.8 eV, consistent with previous reports on Gd_2O_3 materials [1,36]. The obtained bandgap of the SiO_2-PMMA matrix was 4.34 eV. However, when the $Gd_2O_3:Eu^{3+}$ nanoparticles were added the bandgap obtained decreases to 4.05 eV. This reduction in bandgap may be attributed to the presence of larger polymer chains in the doped sample, considering that the PMMA bandgap has been reported between 3.6 and 3.9 eV [37]. Additionally, previous studies indicated that the bandgap of the SiO_2-PMMA matrix can vary based on modifications to its composition [38].

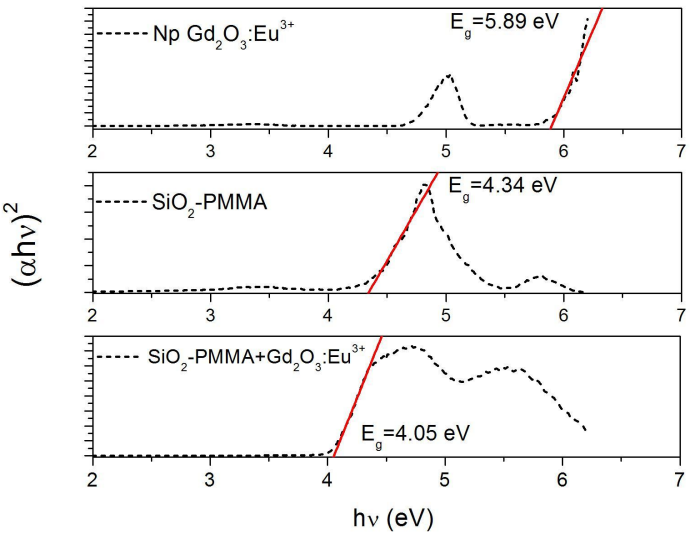

Figure 6. Tauc's formula $(\alpha h\nu)^2$ vs. photon energy for the SiO_2-PMMA samples with and without $Gd_2O_3:Eu^{3+}$ nanoparticles.

Figure 7 shows the photoluminescence spectra for the $Gd_2O_3:Eu^{3+}$ nanoparticles as well as the composite material. The emission from Eu^{3+} ions is evident in the nanoparticles, and this luminescence is retained when the nanoparticles are incorporated into the matrix. The prominent emission peaks occurred at 570, 585, 590, 596, 609, and 627 nm. The highest emission peak is observed at 609 nm, corresponding to the $^5D_0$-$^7F_2$ transition of the Eu^{3+} ions.

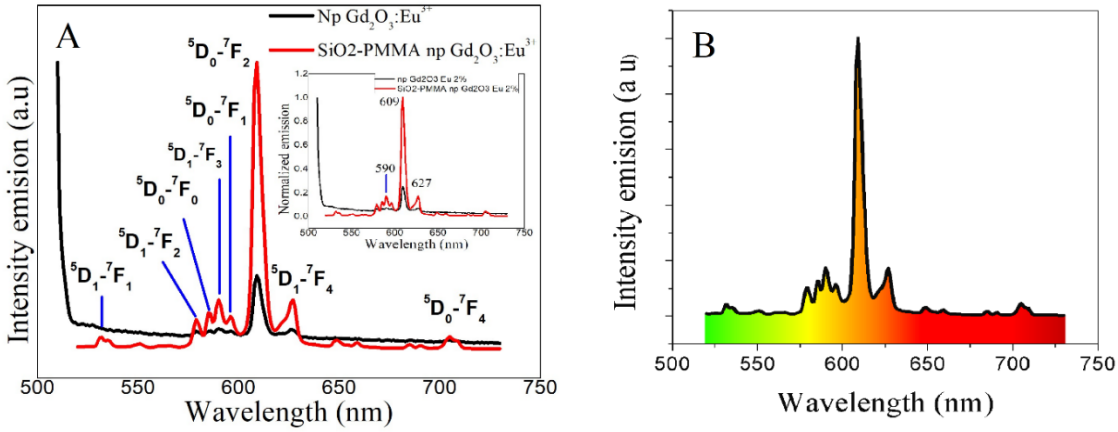

Figure 7. A) Emission spectra of the Gd_2O_3-Eu nanoparticles and the SiO_2-PMMA matrix doped with the nanoparticles. Figure Inset: Normalized emission spectra for the $Gd_2O_3:Eu^{3+}$ nanoparticles, inside and outside the matrix. **B)** Colour emission spectra.

 doi:10.20944/preprints202604.0322.v1

The peaks at 585 and 596 nm are attributed to the $^5D_0$-$^7F_{0,1}$ and $^5D_1$-$^7F_{2,3}$ transitions, respectively, while the peaks at 570 and 590 nm are associated with the transitions $^5D_1$-$^7F_2$ and $^5D_1$-$^7F_3$ [39–41]. The presence of the transitions $^5D_1$-$^7F_{2,3}$, which occur only under certain conditions, suggests that the Eu^{3+} ions occupied vacancies within the Gd_2O_3 structure [13]. Additionally, it is noted that the composite exhibits a higher emission intensity compared to the pure Gd_2O_3:Eu^{3+} nanoparticles. This increased absorption in the UV range along with the enhanced emission from the doped matrix may be explained by the morphology of the material. The SiO_2-PMMA matrix separates the Gd_2O_3:Eu^{3+} clusters, allowing the incident radiation to penetrate deeper into the material. This separation also facilitates the escape of the emitted light from the composite.

Figure 8 presents the CIE chromaticity diagram for the emission of the composite, comparing the emission of the Gd_2O_3:Eu^{3+} nanoparticles when integrated into the SiO_2-PMMA hybrid matrix and shows a slight change in color in the reddish/orange region observed when the nanoparticles are incorporated into the matrix, and is the same color of the normalized emission spectra of the Gd_2O_3:Eu^{3+} nanoparticles and the Gd_2O_3:Eu^{3+} + SiO_2-PMMA composite as shown in Figure 7 (B). The material properties mentioned throughout this work are related to the detection of radiation, having the material in the form of a monolith or even in the form of an optical fiber [42] forming waveshifter optical fibers.

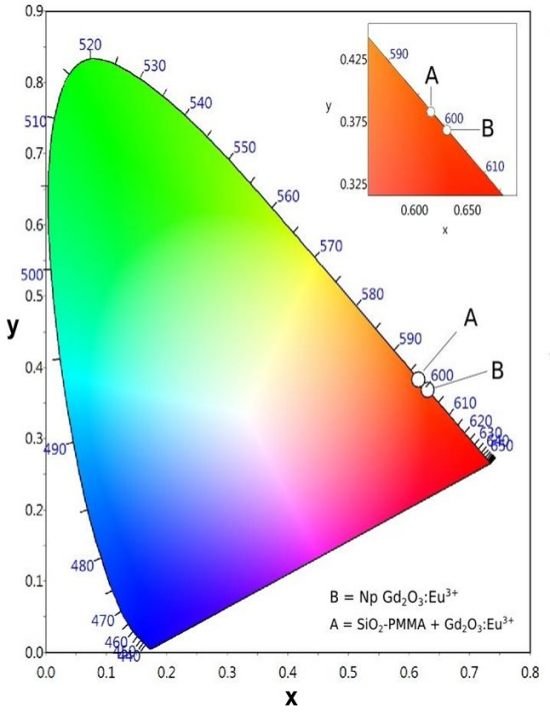

Figure 8. CIE 1931 chromaticity diagram, highlighting their presence inside and outside the matrix, for **A**: Gd_2O_3:Eu^{3+} nanoparticles and **B**: Gd_2O_3:Eu^{3+} + SiO_2-PMMA composite. A zoomed-in section of the graph is shown in the inset.

5. Conclusions

A SiO_2-PMMA hybrid material modified with Gd_2O_3:Eu^{3+} nanoparticles was synthesized using the sol-gel technique. The nanoparticles were successfully integrated into the SiO_2-PMMA matrix without losing their properties, resulting in a luminescent composite. However, a homogeneous solid could not be obtained because most of the nanoparticles precipitated during the drying process of the samples. Instead, the nanoparticles formed a high concentration layer, held together by the SiO_2-PMMA material, while the remainder of the matrix contained a lower concentration of nanoparticle. Although the composite did not behave as initially intended, other beneficial effects were observed that could be useful for multiple applications. Our results indicate that the nanoparticles formed

 doi:10.20944/preprints202604.0322.v1

luminescent clusters within the transparent matrix, which enhanced some of the optical properties of the composite. Additionally, the nanoparticles exposed to the ambient atmosphere exhibited high luminescence, a characteristic that could be advantageous in developing sensors. The thickness of the layers could also be easily controlled by adjusting the ratio between the matrix and the nanoparticles. Nonetheless, more research is needed to understand the interactions between the SiO_2-PMMA matrix gel and the $Gd_2O_3:Eu^{3+}$ nanoparticles, as a similar phenomenon could be leveraged to design other innovative materials.

References

1. Priya, R., Pandey, O. P., & Dhoble, S. J. (2021). Review on the synthesis, structural and photo-physical properties of Gd2O3 phosphors for various luminescent applications. Optics and Laser Technology, 135(October 2020), 106663. https://doi.org/10.1016/j.optlastec.2020.106663.
2. G.H. Lee, Y. Chang, T.J. Kim, "7 - Thermal neutron capture therapy (NCT)," in *Ultrasmall Lanthanide Oxide Nanoparticles for Biomedical Imaging and Therapy*. Woodhead Publishing, 2014, Pages 97-102, doi.org/10.1533/9780081000694.97
3. A.C. Rivera, N.N. Glazener, N.C. Cook, B.A. Akins, J.B. Plumley, N.J. Withers, K. Carpenter, G.A. Smolyakov, R.D. Busch, M. Osiński, "Detection of thermal neutrons using gadolinium-oxide-based nanocrystals," in *Chemical, Biological, Radiological, Nuclear, and Explosives (CBRNE) Sensing XII, April 26-28 2011*, Orlando Fl. USA, A.W. Fountain, P.J. Garderner Eds. SPIE Proceedings, 2011, 80180F, doi.org/10.1117/12.883646
4. QB. Li, J.M. Lin, J.H. Wu, L. Zhang, J.L. Wang, Y. Wang, F. Peng, M.L. Huang, Y.M. Xiao, "Preparation of Gd2O3:Eu3+ downconversion luminescent material and its application in dye-sensitized solar cells", *Chin Sci Bull*, 2011, 56:3114–3118, doi.org/10.1007/s11434-011-4664-z
5. J.S. Kumar, B. Ranganathan, D. Sastikumar, "Ammonia gas sensing property of gadolinium oxide using fiber optic gas sensor", *DAE Solid State Physics Symposium, 26–30 December 2016* Bhubaneswar, Odisha, India, S. Bhattacharya, S. Singh, A. Das, S. Basu Eds. AIP Conference Proceedings No. 1832, 2017, 050119, doi.org/10.1063/1.4980352
6. S. Chaudhary, S. Kumar, A. Umar, J. Singh, M. Rawat, et al., "Europium-doped gadolinium oxide nanoparticles: A potential photoluminescencent probe for highly selective and sensitive detection of Fe^{3+} and Cr^{3+} ions," *Sensors and Actuators B: Chemical*, 2017, 243: 579-588, doi.org/10.1016/j.snb.2016.12.002
7. L. Zhou, Z. Gu, X. Liu, W. Yin, G. Tian, L. Yan, et al. "Size-tunable synthesis of lanthanide-doped Gd_2O_3nanoparticles and their applications for optical and magnetic resonance imaging," *J Mater Chem*, 2012, 22:966–974, doi.org/10.1039/C1JM13758A
8. W. Di, X. Ren, H. Zhao, N. Shirahata, Y. Sakka, et al. "Single-phased luminescent mesoporous nanoparticles for simultaneous cell imaging and anticancer drug delivery," *Biomaterials*, 2011, 32:7226–7233, doi.org/10.1016/j.biomaterials.2011.06.019
9. W.O. Gordon, J.A. Carter, B.M. Tissue, "Long-lifetime luminescence of lanthanide-doped gadolinium oxide nanoparticles for immunoassays," *J Lumin*, 2004, 108:339–342, doi.org/10.1016/j.jlumin.2004.01.071
10. N.M. Maalej, A. Qurashi, A.A. Assadi, R. Maalej, M.N. Shaikh, et al. "Synthesis of Gd_2O_3:Eu nanoplatelets for MRI and fluorescence imaging," *Nanoscale Res Lett*, 2015, 10: 215, doi.org/10.1186/s11671-015-0905-4
11. C. Bouzigues, T. Gacoin, A. Alexandrou, "Biological application of rare-earth based nanoparticles," *ACS Nano*, 2011, 5: 8488–8505, doi.org/10.1021/nn202378b
12. B.G. Yust, D.K. Sardar, L.C. Mimun, A.K. Gangadharan, A.T. Tsin, "Rare earth doped nanoparticles in imaging and PDT", in SPIE BiOS, 19 February 2013, San Francisco, CA, USA, A.N. Cartwright, D.V. Nicolau Eds. Proc. SPIE 8594, 2013, 85940D doi.org/10.1117/12.2004939
13. N. Dhananjaya, H. Nagabhushana, S.C. Sharma, B. Rudraswamy, C. Shivakumara, et al. "Hydrothermal synthesis of $Gd_2O_3:Eu^{3+}$ nanophosphors: Effect of surfactant on structural and luminescence properties," *J Alloys Compd*, 2014, 587:755–762, doi.org.10.1016/J.JALLCOM.2013.10.121
14. F. Mammeri, E. Le Bourhis, L. Rozes, C. Sanchez, "Mechanical properties of hybrid organic–inorganic materials," *J Mater Chem*, 2005, 15:3787-3811, doi.org/10.1039/B507309J

 doi:10.20944/preprints202604.0322.v1

15. M.E. Launey, E. Munch, D.H. Alsem, H.B. Barth, E. Saiz, et al. "Designing highly toughened hybrid composites through nature-inspired hierarchical complexity," *Acta Materialia*, 2009, 57:2919-2932, doi.org/10.1016/j.actamat.2009.03.003
16. M.D. Morales-Acosta, C.G. Alvarado-Beltrán, M.A. Quevedo-López, B.E. Gnade, A. Mendoza-Galván, et al. "Adjustable structural, optical and dielectric characteristics in sol–gel PMMA–SiO2 hybrid films," *J Non-Cryst Solids*, 2013, 362:124-135, doi.org/10.1016/j.jnoncrysol.2012.11.025
17. M. Oubaha, P. Etienne, S. Calas, P. Coudray, J.M. Nedelec, et al. "Sol-Gel derived organic and inorganic hybrid materials for photonic applications: contribution to the correlation between the material structure and the transmission in the near infrared region," *J Sol-Gel Sci Technol*, 2005, 33:241, doi.org/10.1007/s10971-005-5619-0
18. M. Shahbazi, A. Bahari, S. Ghasemi, "Studying saturation mobility, threshold voltage, and stability of PMMA-SiO2-TMSPM nano-hybrid as OFET gate dielectric," *Synth Met*, 2016, 221:332-339, doi.org/10.1016/j.synthmet.2016.09.007
19. M.D. Morales-Acosta, M.A. Quevedo-López, R. Ramírez-Bon, "PMMA–SiO2 hybrid films as gate dielectric for ZnO based thin-film transistors," *Mater Chem Phys*, 2014, 146:380-388, doi.org/10.1016/j.matchemphys.2014.03.042
20. J. Lima-Gutiérrez, R. Palomino-Merino, M.L. Arroyo Carrasco, E. Rubio-Rosas, V.M. Castaño, "Nonlinear optical properties of a MMA-silica nanohybrid material doped with rhodamine 6g," *J Nanomater*, 2013, 2013:1-5, Article ID 374185279-284, doi.org/10.1155/2013/374185
21. T.H. Nhung, M. Canva, T.T.A. Dao, F. Chaput, A. Brun, et al., "Stable Doped Hybrid Sol-Gel Materials for Solid-State Dye Laser," *Appl Opt*, 2003, 42:2213-2218, doi.org/10.1364/ao.42.002213
22. H.A.S. Al-shamiri, I.M. Azzouz, M.S. Shafik, "Photostability and amplified spontaneous emission in dye-activated new organic-inorganic hybrid material," *J Sol-Gel Sci Technol*, 2006, 41:65-69, doi.org/10.1007/s10971-006-0113-x
23. L. Xu, Y.F. Ma, K.Z. Tang, Y. Tan, W.S. Liu, et al. "Preparation, characterization and photophysical properties of highly luminescent terbium complexes incorporated into SiO2/polymer hybrid material," *J Fluoresc*, 2008, 18:685-693, doi.org/10.1007/s10895-008-0344-z
24. N. Hussain, I. Ayoub, U. Mushtaq, R. Sehgal, S. Rubab, R Sehgal, H. C. Swart and V. Kumar "Introduction to phosphors and luminescence," Rare-Earth-activated Phosphors, Ed Elsevier, Chapter 8 pp.3-41, 2022, doi.org/10.1016/B978-0-323-89856-0.00008-0
25. Joint Committee on Powder Diffraction Standards, Diffraction Data File, No.12-797, JCPDF International Center for Diffraction Data, Pennsylvania, 1991.
26. R.D.L. Gaspar et al./Colloids and Surfaces A: Physicochem. Eng. Aspects, 2010, 367:155–160. doi:10.1016/j.colsurfa.2010.07.03
27. S. Hazarika, N. Paul, D. Mohanta, "Rapid hydrothermal route to synthesize cubic-phase gadolinium oxide nanorods," *Bull Mater Sci*, 2014, 37:789–796, doi.org/10.1007/s12034-014-0007-4
28. H. Aguiar, J. Serra, P. González, B. León, "Structural study of sol–gel silicate glasses by IR and Raman spectroscopies," *J Non-Cryst Sol*, 2009, 355:475-480, doi.org/10.1016/j.jnoncrysol.2009.01.010
29. K.J. Thomas, M. Sheeba, V.P.N. Nampoori, C.P.G. Vallabhan, P. Radhakrishnan, "Raman spectra of polymethyl methacrylate optical fibres excited by a 532 nm diode pumped solid state laser," *J Opt A: Pure Appl Opt*, 2008, 10:055303, doi.org/10.1088/1464-4258/10/5/055303
30. J. Yang, J. Chen, J. Song, "Studies of the surface wettability and hydrothermal stability of methyl-modified silica films by FT-IR and Raman spectra," *Vib Spectrosc*, 2009, 50:178-184, doi.org/10.1016/j.vibspec.2008.09.016
31. I. Artaki, M. Bradley, T.W. Zerda, J. Jonas, "NMR and Raman study of the hydrolysis reaction in sol-gel processes," *J Phys Chem*, 1985, 89:4399-4404, doi.org/10.1021/J100266A050
32. J. Dybal, S. Krimm, "Normal-mode analysis of infrared and Raman spectra of crystalline isotactic poly(methyl methacrylate)," *Macromolecules*, 1990, 23:1301-1308, doi.org/10.1021/ma00207a013
33. X. Li, T.A. King, "Microstructure and optical properties of PMMA/gel silica glass composites," *J Sol-Gel Sci Technol*, 1995, 4:75-82, doi.org/10.1007/BF00486705

 doi:10.20944/preprints202604.0322.v1

34. X. Xu, H. Ming, Q. Zhang, Y. Zhang, "Properties of Raman spectra and laser-induced birefringence in polymethyl methacrylate optical fibres," *J Opt A: Pure Appl Opt*, 2002, 4:237-242, doi.org/10.1088/1464-4258/4/3/303
35. E. H. El-Kalla, S. M. Sayyah, H. H. Afifi, A. F. Saeed, "Ultraviolet-visible spectroscopic studies of poly(methyl methacrylate) doped with some luminescent materials," *Acta Polymerica*, 1989, 40:349-351, doi.org/10.1002/actp.1989.010400512
36. Yu A Kuznetsova and A F Zatsepin, "Optical properties and energy parameters of Gd_2O_3 and Gd_2O_3:Er nanoparticles," *J. Phys.: Conf. Ser.*, 2017, 917:062001, doi.org/10.1088/1742-6596/917/6/062001
37. L. N. Ismail, H. Zulkefle, H.H. Sukreen, M. Rusop, "Influence of doping concentration on dielectric, optical, and morphological properties of PMMA thin films," Adv Mat Sci Eng 2012, 2012:1-5, ID 605673, doi.org/10.1155/2012/605673
38. P.M. Trejo-García, R. Palomino-Merino, J. De la Cruz, J.E. Espinosa, R. Aceves, E. Moreno-Barbosa, O.P. Moreno, "Luminescent properties of Eu^{3+}-doped Hybrid hybrid SiO_2-PMMA material for photonic applications, *Micromachines*, 2018, 9:441-450, doi.org/10.3390/mi9090441
39. K. Binnemans, "Interpretation of Europium(III) spectra," *Coord Chem Rev*, 2015, 295, 1–45, doi.org/10.1016/j.ccr.2015.02.015
40. E. Pavitra, J.S. Yu, "A facile large-scale synthesis and luminescence properties of Gd_2O_3:Eu^{3+} nanoflowers," *Mater Lett*, 2013, 90:134-137, doi.org/10.1016/j.matlet.2012.09.022
41. Y. Wang, X. Bai, T. Liu, B. Dong, L. Xu, Q. Liu, H. Song, "Solvothermal synthesis and luminescence properties of monodisperse Gd_2O_3:Eu^{3+} and Gd_2O_3:Eu^{3+}@SiO_2 nanospheres, *J Solid State Chem*, 2010, 183:2779-2785, doi.org/10.1016/j.jssc.2010.09.002
42. W. Bae, J. Cesar, K. Chen, J. Cho, D. Du, J. Edgar, W. Earthman, O.M. Falana, M. Gajda, C. Hurlbut, M. Jackson, K. Lang, C. Lee, J.Y. Lee, E. Liang, J. Liu, C. Maxwell, C. Murthy, D. Myers, S. Nguyen, T. O'Brien, M. Proga, T. Rodriguez, S. Syed, M. Zalikha and J. Zey, "Optical characterization of wavelength-shifting and scintillating-wavelength-shifting fibers", Journal of Instrumentation, 2026, 21:P01027. doi.org/10.1088/1748-0221/21/01/P01027